

Phonon-mediated spin-polarized superconductivity in altermagnets

Kristoffer Leraand,¹ Kristian Mæland,² and Asle Sudbø^{1,*}

¹*Center for Quantum Spintronics, Department of Physics,
Norwegian University of Science and Technology, NO-7491 Trondheim, Norway*

²*Institute for Theoretical Physics and Astrophysics, University of Würzburg, D-97074 Würzburg, Germany*

We consider the possibility of phonon-mediated unconventional superconductivity in a recently discovered new class of antiferromagnets, dubbed altermagnets. Within a weak-coupling approach, and using a minimal Lieb lattice model for altermagnets, we find a dominant superconducting instability odd in momentum and even in spin with spin-polarized Cooper pairs. We discuss the origin of this unusual result in terms of the spin-structure of the altermagnetic Fermi surface, in combination with the momentum-space structure of the effective phonon-mediated electron-electron interactions on the Fermi surface.

I. INTRODUCTION

More than a century after its discovery [1, 2], superconductivity continues to be one of the most intensely studied topics in condensed matter physics, with deep connections to the most fundamental descriptions of matter [3–6]. This macroscopic quantum phenomenon is characterized by zero electrical resistance and Higgs condensation, rendering the photon massive [3, 5, 7] below some critical temperature T_c . Superconductors arising out of good metals with small correlation effects (conventional low- T_c superconductors with a nodeless s -wave superconducting gap), are well described by the Bardeen-Cooper-Schrieffer (BCS) theory [8]. Within BCS theory the phenomenon arises from an instability of the Fermi surface (FS) due to effective attraction between electrons. Originally, exchange of phonons mediated the attraction. The discovery of unconventional superconductivity with nodal gaps in strongly correlated fermion systems such as heavy fermions [9, 10] and high- T_c superconductivity [11–15] highlighted that other bosons could also be responsible for the pairing. In unconventional superconductors [16], the pairing mechanism often involves complex interactions, such as spin fluctuations, electronic correlations, or orbital effects, leading to non-trivial symmetry and momentum-dependent superconducting gaps. In the high- T_c cuprates, nodes in the gap on the FS have been established through phase-sensitive measurements [17], establishing that the gap is spin-singlet with $d_{x^2-y^2}$ -wave symmetry. Furthermore, low- T_c , possibly p -wave, spin-triplet pairing in itinerant ferromagnets has been predicted and observed [18–22]. Finally, magnon-mediated unconventional superconductivity in heterostructures of magnetic insulators and various gapless fermionic systems has been considered extensively [23–37].

Recently, altermagnets have emerged as a new class of magnetic materials that defy the traditional dichotomy of collinear ferromagnetism and antiferromagnetism [38–50]. Altermagnets exhibit time-reversal symmetry breaking and spin-split band structures, yet maintain compensated magnetic ordering without net magnetization. They combine properties of ferromagnets and antiferromagnets, opening new avenues for

superconductivity research [39, 51–58]. Importantly, the spin-split electronic bands in altermagnets exhibit symmetries that can support exotic pairing states [59] in the presence of suitable interactions. However, spin-singlet or mixed-spin spin-triplet superconductivity requires finite-momentum Cooper pairs or odd-frequency superconductivity [54, 55, 60]. Even-frequency zero-momentum Cooper-pairing requires fully spin-polarized Cooper pairs.

Previously, unconventional magnon-mediated superconductivity has been investigated in a minimal model of altermagnets [39, 58] on a Lieb lattice [61–65]. This particular model exhibits antiferromagnetism along with $d_{x^2-y^2}$ -wave symmetric spin splitting of the electron bands. The existence of altermagnetism in Lieb lattices has also been confirmed using Hubbard models [66, 67]. While realizing a 2D electronic Lieb lattice has been a longstanding challenge [64, 65], several proposed quasi-two-dimensional (2D) altermagnets display the Lieb lattice in nearly decoupled layers [46–48, 67, 68]. Magnon-mediated superconductivity with zero-momentum Cooper-pairs in altermagnets, requires invoking double-magnon processes to obtain superconductivity [39, 58]. In a strong-coupling superconductivity scenario, many-body effects on this superconductivity has been investigated [58] using Eliashberg theory of strong-coupling superconductivity [69, 70]. In this case, strong-coupling renormalizations leads to substantial suppression of the critical temperature T_c [58]. Were the electron-electron interaction to be mediated by a spinless boson, the necessity of a double-boson mediated interaction would be obviated, and the strong-coupling reduction of T_c possibly avoided.

The potential of phonons to yield unconventional superconductivity has been explored in spin-orbit coupled systems, though s -wave spin-singlet pairing seems to be preferred from phonons alone [71]. Ref. [72] considers a situation where both phonons and spin fluctuations contribute to d -wave pairing. More recently, it has been demonstrated that by including vertex corrections, phonons may mediate d -wave spin-singlet in strong-coupling superconductors [73].

In this work, we predict the emergence of unconventional *fully spin-polarized* superconductivity in altermagnets mediated by electron-phonon interactions. The examples mentioned above of phonon-mediated conventional and unconventional spin-singlet superconductivity are not an option in the spin-split band structure of altermagnets, at least not for zero-momentum

* asle.sudbo@ntnu.no

Cooper-pairs. Spin-polarized supercurrents are attractive for the field of superconducting spintronics [74], usually realized in complicated heterostructures relying on proximity induced superconductivity. We propose that spin polarized phonon-mediated superconductivity can arise intrinsically in altermagnets. Our result originates from the interplay between spin-symmetries of the electron bands in altermagnets, and the momentum dependence of the electron-phonon interaction. This provides a new pathway for realizing unconventional superconductivity via a conventional mechanism, and with a substantial T_c .

II. PHONON MODEL

The phonon energies and mode vectors can be found by considering the eigenvalue equation [75–78]

$$\sum_{\beta} D_{\mathbf{q}}^{\alpha\beta} \hat{e}_{\mathbf{q}\beta}^{\lambda} = M_{\alpha} \omega_{\mathbf{q}\lambda}^2 \hat{e}_{\mathbf{q}\alpha}^{\lambda}, \quad (1)$$

where $\alpha, \beta \in \{1, 2, 3\}$ label the three atoms in the Lieb lattice basis illustrated in Fig. 1 (a), referring to the spin-up, non-magnetic, and spin-down sublattices respectively. D is the dynamical matrix, which is the Fourier transformation of the force constant matrix (FCM). The phonon modes are indicated by λ , $\hat{e}_{\mathbf{q}}$ is the normalized vector of the Fourier transformed displacement vector, \mathbf{q} is the momentum of the phonon, M_{α} is the mass of atom α , and $\omega_{\mathbf{q}\lambda}$ is the phonon frequency. The symmetries of the Lieb lattice, given in App. A, constrain the elements of the FCM [39], leaving 11 free parameters. As shown in App. B, by applying additional constraints, we are able to relate these parameters and are only left with one free parameter, η . This parameter will only affect the phonon bandwidth, which we have chosen to be around 30 meV. As shown in App. C, in our first-order electron-phonon coupling in a 2D system, only the in-plane (IP) phonon modes will couple to the electrons, as such, we discard the out-of-plane (OOP) modes. The IP bands are shown in Fig. 1 (b).

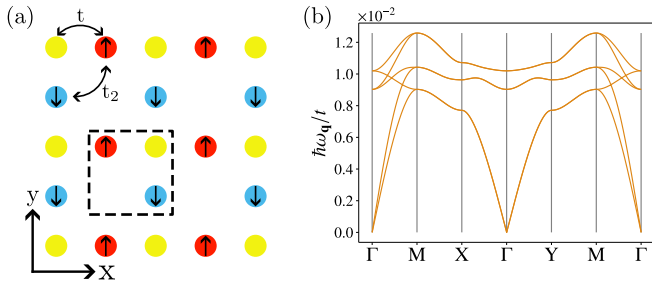


FIG. 1. (a) The Lieb lattice, where the black square indicates the chosen unit cell, which contains three atoms with different localized spins, namely, spin-up (red), non-magnetic (yellow), and spin-down (blue). (b) The IP phonon bands for the Lieb lattice on a path between the symmetry points of the Brillouin zone, see Tab. I for the parameter values used.

III. ELECTRON MODEL

We utilize a minimal model of a Lieb lattice [61, 66, 67] to describe altermagnetic behavior, where itinerant electrons can hop between nearest-neighbor (NN)- and next-nearest-neighbor (NNN) sites, as well as interact with the localized spins on these sites. The electronic tight-binding Hamiltonian of the model is given by [39]

$$H_{\text{el}} = t \sum_{\langle i,j \rangle \sigma} c_{i\sigma}^{\dagger} c_{j\sigma} + t_2 \sum_{\langle\langle i,j \rangle\rangle \sigma} c_{i\sigma}^{\dagger} c_{j\sigma} - J_{\text{sd}} \sum_{i\sigma\sigma'} \mathbf{S}_i \cdot c_{i\sigma}^{\dagger} \boldsymbol{\sigma}_{\sigma\sigma'} c_{i\sigma'} - \mu \sum_{i\sigma} c_{i\sigma}^{\dagger} c_{i\sigma}, \quad (2)$$

where $c_{i\sigma}^{(\dagger)}$ annihilates (creates) an electron with spin σ at site i . The pairs $\langle i, j \rangle$ and $\langle\langle i, j \rangle\rangle$ denote nearest- and next-nearest neighbors with hopping amplitudes t and t_2 , respectively. J_{sd} is the on-site exchange coupling between the itinerant electrons and the localized spins \mathbf{S}_i , and $\boldsymbol{\sigma}$ is the vector consisting of Pauli matrices. The spins \mathbf{S}_i have a length S , and the on-site energy is set by the chemical potential μ . We assume that spin-orbit coupling is negligible compared to the spin-splitting.

The electronic energy spectrum obtained from this Hamiltonian is showcased in Fig. 2 (a), which exhibits the characteristic $d_{x^2-y^2}$ -wave spin-split electron bands of an altermagnet. The key feature when finding the spin-polarized superconductivity is the existence of regions that are completely spin-split for all momenta, which can be observed between the middle and top bands. To obtain this spectrum, we diagonalize the Hamiltonian in momentum space as $H_{\text{el}} = \sum_{n\mathbf{k}\sigma} \varepsilon_{n\mathbf{k}\sigma} d_{n\mathbf{k}\sigma}^{\dagger} d_{n\mathbf{k}\sigma}$, where $\varepsilon_{n\mathbf{k}\sigma}$ is the energy of band n for excitations with momentum \mathbf{k} and spin σ , while $d_{n\mathbf{k}\sigma}^{(\dagger)}$ are the annihilation (creation) band operators. These operators are related to the electron operators as $d_{n\mathbf{k}\sigma} = \sum_{\alpha} q_{\mathbf{k}\sigma\alpha n}^* c_{\mathbf{k}\sigma\alpha}$, where α indicates the different atoms in the basis, and the coefficient $q_{\mathbf{k}\sigma\alpha n}$ is the component α in the eigenvector of the Hamiltonian corresponding to band n .

Due to the $d_{x^2-y^2}$ -wave symmetry of the spin splitting, spin-up and spin-down bands are interchangeable by a rotation of 90° in momentum space. Hence, all properties of the two spins are connected by this rotation. To showcase the role of

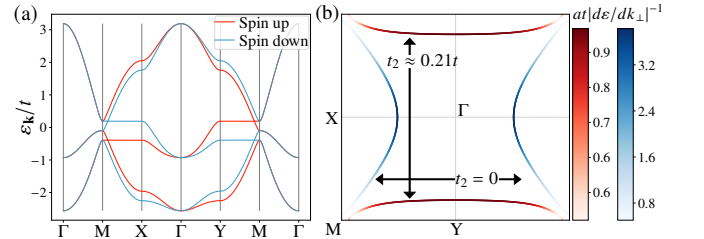


FIG. 2. (a) The electronic band structure along a high-symmetry path in the BZ for $\mu = 0$. (b) The FSs for spin-up (red) and spin-down (blue), the colors indicate $at|d\varepsilon/dk_{\perp}|^{-1}$ for $\mu = 0.1t$. The NNN hopping is $t_2 \approx 0.21t$ for spin-up, and $t_2 = 0$ for spin-down. This particular system exhibits altermagnetism with $d_{x^2-y^2}$ -wave spin splitting. See Tab. I for the rest of the parameters used.

NNN hopping, we present the results with a NNN hopping of $t_2 \approx 0.21t$ for spin-up electrons and the results with $t_2 = 0$ for spin-down electrons throughout the paper. The electronic band structure for $t_2 = 0$ can be found in Ref. [39].

IV. ELECTRON-PHONON COUPLING

The electron-phonon interaction is found by an expansion of the two hopping amplitudes in Eq. (2) to first order of displacements away from equilibrium, similar to Ref. [79].

$$t(\mathbf{r}_{i\alpha j\beta}) \approx t(\boldsymbol{\delta}) + \mathbf{u}_{ij\alpha\beta} \cdot \nabla_r t(\mathbf{r}_{i\alpha j\beta}) \Big|_{\mathbf{r}_{i\alpha j\beta}=\boldsymbol{\delta}}, \quad (3)$$

where $\mathbf{r}_{i\alpha j\beta}$ is the instantaneous separation between atoms $i\alpha$ and $j\beta$, $\boldsymbol{\delta}$ are vectors connecting the atoms in equilibrium, and $\mathbf{u}_{ij\alpha\beta}$ is their relative displacement from equilibrium. ∇_r denotes the gradient with respect to $\mathbf{r}_{i\alpha j\beta}$, and $|_{\mathbf{r}_{i\alpha j\beta}=\boldsymbol{\delta}}$ indicates to evaluate the atom positions in equilibrium. See App. C for the full derivation of the electron-phonon coupling. The first term of Eq. (3) is the equilibrium hopping used in Eq. (2), while the second term is the source of the electron-phonon interaction. We quantize the displacements as [75, 76]

$$\mathbf{u}_{i\alpha} = \sum_{\mathbf{q}\lambda} \sqrt{\frac{\hbar}{2M_\alpha N \omega_{\mathbf{q}\lambda}}} \hat{\mathbf{e}}_{\mathbf{q}\alpha}^\lambda (a_{-\mathbf{q},\lambda}^\dagger + a_{\mathbf{q},\lambda}) e^{-i\mathbf{q}\cdot\mathbf{R}_{i\alpha}}, \quad (4)$$

where $a_{\mathbf{q}\lambda}^{(\dagger)}$ annihilates (creates) a phonon with momentum \mathbf{q} in mode λ , N is the number of unit cells, and $\mathbf{R}_{i\alpha}$ is the equilibrium position of atom α in unit cell i .

By substituting Eq. (3) in Eq. (2), as well as utilizing the band operators, we find the electron-phonon interaction

$$H_{\text{el-ph}} = \sum_{\mathbf{k}\mathbf{q}\sigma\lambda} g_{\sigma\lambda}(\mathbf{k}, \mathbf{k} + \mathbf{q}) (a_{-\mathbf{q},\lambda}^\dagger + a_{\mathbf{q},\lambda}) d_{\mathbf{k}+\mathbf{q},\sigma}^\dagger d_{\mathbf{k},\sigma}, \quad (5)$$

where the electron-phonon coupling strength is given by

$$\begin{aligned} g_{\lambda\sigma}(\mathbf{k}, \mathbf{k} + \mathbf{q}) &= g_{\lambda\sigma}^{(1)}(\mathbf{k}, \mathbf{k} + \mathbf{q}) + g_{\lambda\sigma}^{(2)}(\mathbf{k}, \mathbf{k} + \mathbf{q}), \\ g_{\lambda\sigma}^{(j)}(\mathbf{k}, \mathbf{k} + \mathbf{q}) &= \frac{t_j}{2} \sqrt{\frac{\hbar}{2N\omega_{\mathbf{q}\lambda}}} \sum_{\alpha\beta} q_{\mathbf{k}+\mathbf{q},\sigma\alpha}^* q_{\mathbf{k}\sigma\beta} \\ &\times \sum_{\delta_j} e^{i\mathbf{k}\cdot\boldsymbol{\delta}_j} \left(\frac{\delta_{jx}}{\sigma_x^2}, \frac{\delta_{jy}}{\sigma_y^2} \right) \cdot \left[\frac{\hat{\mathbf{e}}_{\mathbf{q}\beta}^\lambda}{\sqrt{M_\beta}} e^{i\mathbf{q}\cdot\boldsymbol{\delta}_j} - \frac{\hat{\mathbf{e}}_{\mathbf{q}\alpha}^\lambda}{\sqrt{M_\alpha}} \right], \end{aligned} \quad (6)$$

where $j \in \{1, 2\}$ indicates whether it is the NN or the NNN coupling, and σ_x, σ_y are the standard deviations of the atomic orbitals. Note that we have omitted the band indices, as we consider the scattering to be confined to the FS.

V. SUPERCONDUCTIVITY

Next, we transform the electron-phonon interaction into an effective electron-electron interaction by applying a Schrieffer-

Wolff transformation [80, 81], see App. C for the full derivation, will,

$$H_{\text{eff}} = \frac{1}{2} \sum_{\mathbf{k}\mathbf{k}'\sigma} \bar{V}_{\mathbf{k}'\mathbf{k}\sigma} d_{\mathbf{k}'\sigma}^\dagger d_{-\mathbf{k}',\sigma}^\dagger d_{-\mathbf{k},\sigma} d_{\mathbf{k}\sigma}, \quad (7)$$

where we have followed Refs. [34, 58], and symmetrized the effective interaction as $2\bar{V}_{\mathbf{k}'\mathbf{k}\sigma} \equiv V_{\mathbf{k}'\mathbf{k}\sigma} + V_{-\mathbf{k}',-\mathbf{k}\sigma} - V_{-\mathbf{k}',\mathbf{k}\sigma} - V_{\mathbf{k}',-\mathbf{k}\sigma}$, with the effective electron-electron interaction on the FS of spin σ , $V_{\mathbf{k}'\mathbf{k}\sigma}$ given by

$$V_{\mathbf{k}'\mathbf{k}\sigma} = - \sum_{\lambda} \frac{g_{\lambda\sigma}(\mathbf{k}, \mathbf{k}') g_{\lambda\sigma}(-\mathbf{k}, -\mathbf{k}')}{\hbar\omega_{\mathbf{k}'-\mathbf{k},\lambda}}. \quad (8)$$

As shown in Refs. [39, 58] the electrons have the greatest DOS for $-J_{\text{sd}}S < \mu < J_{\text{sd}}S$ so we expect the greatest T_c here. In the region $0 < \mu < J_{\text{sd}}S$, there is no overlap of the spin up and spin down FSs, also with $t_2 \neq 0$. Hence, spin-singlet zero-momentum pairing is ruled out, and we focus on this region. The most likely scenario with the type of FS of our model appears to be zero-momentum pairing. This provides the greatest possible phase space for interactions, and, unlike other models, there is a very small overlap of the spin up and spin down FSs even with a finite momentum, App. E. Hence, we look for spin-triplet pairing, which necessitates odd-parity gap functions, and hence an odd-parity symmetrized coupling [16, 34]. The symmetrized interaction is shown in Fig. 3 (a) and depicts a p -wave symmetry.

We consider weak-coupling superconductivity and apply the linearized BCS equation to solve for the spin-polarized superconducting gap $\Delta_{\mathbf{k}\sigma}$ and critical temperature. Since electrons close to the FS dominate the superconducting pairing, we utilize the FS average of the BCS equation [39, 58, 82, 83]

$$\lambda \Delta_{k_{\parallel}\sigma} = - \frac{N S_{\text{FS}}}{A_{\text{BZ}} N_{\text{samp}}} \sum_{k'_{\perp}} \left| \frac{d\varepsilon}{dk'_{\perp}} \right|^{-1} \bar{V}_{k_{\parallel}k'_{\perp}\sigma} \Delta_{k'_{\perp}\sigma}, \quad (9)$$

where S_{FS} denotes the length of the FS and A_{BZ} the area of the first Brillouin zone. N_{samp} is the number of sampling points, we split \mathbf{k} into components $(k_{\parallel}, k_{\perp})$ tangent and normal to the FS, with $d\varepsilon/dk'_{\perp}$ being the derivative of the electron energy in the normal direction to the FS.

If we momentarily consider a jellium model for phonons [76], the strength of the electron-phonon coupling depends only on the momentum transfer. Still considering spin-polarized superconductivity, the symmetrized coupling would be $\bar{V}_{\mathbf{k}\mathbf{k}'\sigma} = -|g_{\mathbf{k}-\mathbf{k}'}|^2/\hbar\omega_{\mathbf{k}-\mathbf{k}'} + |g_{\mathbf{k}+\mathbf{k}'}|^2/\hbar\omega_{\mathbf{k}+\mathbf{k}'}$ on the FS for spin σ .

Let us first consider a simple model for acoustic phonons, $g_{\mathbf{q}} = g\sqrt{|\mathbf{q}|}$ and $\omega_{\mathbf{q}} = u|\mathbf{q}|$. Then, $|g_{\mathbf{q}}|^2/\hbar\omega_{\mathbf{q}} = g^2/\hbar u$ is momentum independent, and so $\bar{V}_{\mathbf{k}\mathbf{k}'\sigma} = 0$. There is no phonon-mediated spin-polarized Cooper pairing from acoustic phonons within such a simple continuum model. Next, consider a simple model of Einstein phonons, $g_{\mathbf{q}} = g|\mathbf{q}|$ and $\omega_{\mathbf{q}} = \omega_E$. Then, $\bar{V}_{\mathbf{k}\mathbf{k}'\sigma} = g^2(|\mathbf{k} + \mathbf{k}'|^2 - |\mathbf{k} - \mathbf{k}'|^2)/\hbar\omega_E$. Imagining an approximately circular FS around the Γ point, the symmetrized interaction closely resembles $\bar{V}_{\mathbf{k}\mathbf{k}'\sigma} = V \cos \phi_{\mathbf{k}\mathbf{k}'}$, with $\phi_{\mathbf{k}\mathbf{k}'}$ being the angle between \mathbf{k} and \mathbf{k}' , and $V > 0$ some positive energy. When solving the eigenvalue problem in Eq. (9)

for a positive eigenvalue λ , it is advantageous for the interaction to be attractive when \mathbf{k}' is close to \mathbf{k} , due to the negative sign on the RHS. A coupling of the form $\bar{V}_{\mathbf{k}\mathbf{k}'\sigma} = V \cos \phi_{\mathbf{k}\mathbf{k}'}$ with $V > 0$ prevents non-trivial gap solutions, since the strongest coupling is always at $\mathbf{k} = \pm\mathbf{k}'$, with a disadvantageous sign. This illustrates the key difference between phonon- and magnon-mediated interactions, since for magnons typically $|g_{\mathbf{k}-\mathbf{k}'}| > |g_{\mathbf{k}+\mathbf{k}'}|$ when $\mathbf{k} \approx \mathbf{k}'$ due to the strength of the interaction increasing for long-wavelength magnons [27]. In contrast, for long-wavelength optical phonons, the coupling tends to vanish. Hence, in simple continuum models, optical phonons are also unlikely to yield spin-polarized superconductivity.

The electron-phonon coupling in Eq. (6) depends on both the incoming and outgoing momentum. The simple forms of $g_{\mathbf{q}}$ and $\omega_{\mathbf{q}}$ of the jellium model are replaced by complex phase factors giving a richer momentum structure on a lattice¹. Thus, both acoustic and optical phonons contribute to the symmetrized pairing, giving a non-zero symmetrized interaction in Fig. 3 (a).

From Fig. 3 (a), the interaction has a similar disadvantageous sign as discussed for jellium optical phonons. However, the interaction is now stronger for $\mathbf{k} \neq \pm\mathbf{k}'$ than at $\mathbf{k} = \pm\mathbf{k}'$, such as in the corners of Fig. 3 (a), which enables solutions for the gap. If at some $\mathbf{k}' \neq \mathbf{k}$ we have $\bar{V}_{k_{\parallel}k'_{\parallel}\sigma} > 0$ and $|\bar{V}_{k_{\parallel}k'_{\parallel}\sigma}| > |\bar{V}_{k_{\parallel}k_{\parallel}\sigma}|$, it is possible to have non-trivial solutions of the gap equation if $\Delta_{\mathbf{k}\sigma}$ and $\Delta_{\mathbf{k}'\sigma}$ have opposite signs, effectively canceling the negative sign on the RHS of Eq. (9). For that reason, our gap solutions tend to have more sign changes on the FS than the effective electron-electron interaction, see Fig. 3.

We are interested in the largest eigenvalue of Eq. (9), λ_m , which is related to the critical temperature by [8]

$$k_B T_c \approx 1.13 \hbar \omega_P e^{-\frac{1}{\lambda_m}}, \quad (10)$$

where ω_P is the largest phonon frequency. Due to the exponential dependence of the critical temperature on the dimensionless coupling, the calculated value of the critical temperature will be sensitive to the chosen values of our parameters. Regardless, our aim is not to pinpoint the exact value of the critical temperature, but rather to show, as a proof of concept, the possibility of achieving finite critical temperatures of phonon-mediated spin-polarized superconductivity. We parameterize the FS similarly to Ref. [39], and ensure we use enough sampling points to get convergence of λ_m to 3 decimals. Fig. 4 (a) shows that when including the NNN hopping, the dimensionless coupling is much larger for low values of the chemical potential compared to the case $t_2 = 0$. Including NNN hopping means that more electrons couple to the phonons. This can be understood by studying the interactions in Fig. 3 (a), where for $t_2 = 0$, the interaction is much weaker around the center of the arcs and stronger in the corners. The matrix elements of the BCS

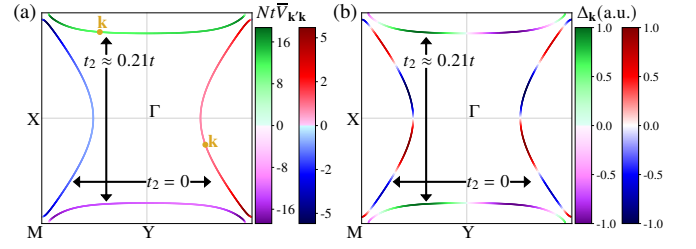


FIG. 3. (a) shows $N\bar{V}_{\mathbf{k}\mathbf{k}'\sigma}$ for both spin-up (green and purple) and spin-down (red and blue). The values for \mathbf{k} are given in yellow and correspond to the maximum of the gap, while the position along the Fermi surface gives \mathbf{k}' . (b) illustrates the normalized superconducting gap in arbitrary units for both spin-up, and spin-down with the same color coding as in (a). In both plots, the chemical potential is set to $\mu = 0.1t$, see Tab. I for the other parameters.

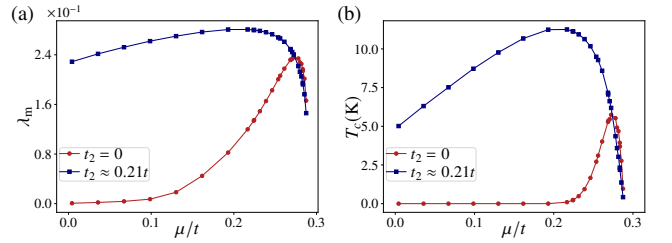


FIG. 4. (a) shows the dimensionless coupling and (b) shows the critical temperature, both as functions of the chemical potential for the two cases of including and excluding NNN hopping. See Tab. I for the parameters used.

equation, Eq. (9), are essentially the interaction multiplied by the inverse slope of the band. Comparing the interaction with the inverse slopes in Fig. 2 (b), the inverse slopes are larger at the center of the arcs and weaker towards the edges. However, for $t_2 \approx 0.21t$, the interaction and the slopes are to a larger degree constant along the arcs, which makes the eigenvalues larger.

The dimensionless coupling, λ_m , decreases as the chemical potential approaches the band crossing at $\varepsilon = J_{sd}S$. As shown in Fig. 2 (b), the bands become increasingly flat when approaching the crossing, especially along the lines ΓX and ΓY , which causes the RHS of Eq. (9) to diverge. Combined with the unfavorable sign of the interaction, this makes it increasingly difficult to satisfy the conditions for a gap with a large eigenvalue.

Careful ARPES measurements of the gap amplitude $|\Delta_{\mathbf{k}}|$ would yield information on the nodal structure of the gap. Combining this with phase-sensitive measurements can corroborate the presence of nodes [17]. Additionally, confirming the presence of nodes using STM based methods has been proposed [84, 85]. If the number of nodes on the FS per spin corresponds to p - or f -wave gaps, it would be a strong indication that the mechanism described in this paper is at play. Note that nodal gaps are sensitive to impurities, and so an experimental realization likely requires a rather clean system. Identification of nodes can, in principle, be used to distinguish zero-momentum spin-triplet pairing from finite-momentum spin-singlet pairing,

¹ The electron transformation coefficients are real and even in momentum and hence only provide quantitative, not qualitative changes of the symmetrized interaction.

since the latter yields *s*-wave or *d*-wave pairing [54, 55]. As noted in Ref. [54], finite momentum pairing is also predicted to yield a distinct Bogoliubov-de Gennes quasiparticle energy spectrum and a distinct density of states compared to zero-momentum pairing. In our case, with a nodal gap, we predict a V-shaped density of states. We emphasize that these predictions should be directly testable on the compounds $\text{Rb}_{1-\delta}\text{V}_2\text{Te}_2\text{O}$, $\text{KV}_2\text{Se}_2\text{O}$, and $\text{La}_2\text{O}_3\text{Mn}_2\text{Se}_2$ [46–48].

VI. CONCLUSION

We have shown that phonon-mediated interactions can lead to unconventional, spin-polarized Cooper pairing with substantial T_c in altermagnets. By analyzing the interplay between the unique band structure of altermagnets and electron-phonon coupling, we have found that the distinct spin-splitting in altermagnetic materials enables a novel superconducting state that is fundamentally different from conventional superconductors. The altermagnetic symmetry allows phonons to mediate spin-polarized pairing. The fully spin-polarized nature of the resulting Cooper pairs represents a significant departure from traditional *s*-wave or spin-singlet superconductivity, offering new possibilities for spintronics and quantum technology applications. Our results further highlight that altermagnetic materials provide a natural platform for exploring unconventional superconducting states, driven by interactions that are traditionally associated with conventional superconductors.

ACKNOWLEDGMENTS

KL and AS were supported by the Research Council of Norway (RCN) through its Centres of Excellence funding scheme, Project No. 262633, “QuSpin”, RCN Project No. 323766, as well as COST Action CA21144 “Superconducting Nanodevices and Quantum Materials for Coherent Manipulation”. KM was supported by the DFG (SFB 1170) and the Würzburg-Dresden Cluster of Excellence ct.qmat, EXC 2147 (Project-Id 390858490).

Appendix A: Lattice symmetries

We model the altermagnet as a two-dimensional Lieb lattice as proposed in Ref. [39], a figure of the lattice can be found in Fig. 1 (a). The Lieb lattice exhibits the eight symmetries

$$\begin{aligned} & (E|0), \quad (C_{2z}|0), \quad (\sigma_x|0), \quad (\sigma_y|0), \\ & (C_{4z}^+|\mathcal{T}), \quad (C_{4z}^-|\mathcal{T}), \quad (\sigma_{xy}|\mathcal{T}), \quad (\sigma_{\bar{x}\bar{y}}|\mathcal{T}), \end{aligned} \quad (\text{A1})$$

where E is the identity operation, C_{2z} is a twofold rotation, C_{4z}^+ and C_{4z}^- are fourfold clockwise and anticlockwise rotations respectively, while σ_x , σ_y , σ_{xy} and $\sigma_{\bar{x}\bar{y}}$ are mirror symmetries about the x -axis, y -axis, the $y = x$ diagonal, and the $y = -x$ diagonal, respectively. \mathcal{T} is the time-reversal operator, effectively flipping the on-site spins. The notation $(A|0)$ means that A is a symmetry without performing time-reversal, while

$(B|\mathcal{T})$ indicates that a combination of B and time-reversal is a symmetry.

Appendix B: Phonon properties from symmetries

The phonon spectrum and eigenmodes are determined in the standard manner by studying the displacements $\mathbf{u}_{i\alpha}$ of the lattice sites from their equilibrium positions $\mathbf{R}_{i\alpha}$, where i refer to the unit cell and α , the different atoms in the basis. We start by expanding the lattice potential around equilibrium, keeping terms up to and including second order in displacements [76, 78]

$$\begin{aligned} V(\mathbf{r}_{11}, \dots, \mathbf{r}_{NN_b}) &= V(\mathbf{R}_{11}, \dots, \mathbf{R}_{NN_b}) \\ &+ \sum_{i\alpha\mu} \left. \frac{\partial V}{\partial r_{i\alpha}^\mu} \right|_{\text{eq}} u_{i\alpha}^\mu + \frac{1}{2} \sum_{i\alpha\mu} \sum_{j\beta\nu} \left. \frac{\partial^2 V}{\partial r_{i\alpha}^\mu \partial r_{j\beta}^\nu} \right|_{\text{eq}} u_{i\alpha}^\mu u_{j\beta}^\nu, \end{aligned} \quad (\text{B1})$$

where $\mathbf{r}_{i\alpha} = \mathbf{R}_{i\alpha} + \mathbf{u}_{i\alpha}$, is the instantaneous position of the lattice atoms, N and N_b denote the number of unit cells and atoms in the basis, respectively. $\mu, \nu \in \{x, y, z\}$ label Cartesian directions, and $|_{\text{eq}}$ denote evaluation at equilibrium. The first term is a constant, which we can ignore, and the second term is a force, yielding zero when evaluated in equilibrium, so we are only left with the third term. We define the coefficient of the last term as the force constant matrix (FCM) $\Phi_{\mu\nu}^{\alpha\beta}(\mathbf{R}_i - \mathbf{R}_j) \equiv \left. \frac{\partial^2 V}{\partial r_{i\alpha}^\mu \partial r_{j\beta}^\nu} \right|_{\text{eq}}$. The FCM is related to the potential of the lattice, hence, it must satisfy the same symmetries as the lattice, namely, Eq. (A1), which allows us to find constraints on the matrix elements of the FCM. In addition to these symmetries, the FCM satisfies the conditions [75, 78]

$$\sum_{j\beta} \Phi_{\mu\nu}^{\alpha\beta}(\mathbf{R}_i - \mathbf{R}_j) = 0, \quad (\text{B2})$$

$$\Phi_{\mu\nu}^{\alpha\beta}(\mathbf{R}_i - \mathbf{R}_j) = \sum_{\mu'\nu'} S_{\mu\mu'}^T \Phi_{\mu'\nu'} [(\mathcal{S}(\mathbf{R}_{i\alpha}) - \mathcal{S}(\mathbf{R}_{j\beta})) S_{\nu'\nu}], \quad (\text{B3})$$

where \mathcal{S} is a symmetry of the lattice, so $\mathcal{S}(\mathbf{R}_{i\alpha})$ is the transformed vector of $\mathbf{R}_{i\alpha}$ under the symmetry, and \mathcal{S} is the matrix representation of this symmetry. We interpret $\Phi^{\alpha\beta}(\mathbf{R}_i - \mathbf{R}_j)$ as a bond between atom $i\alpha$ and atom $j\beta$, and separate the symmetries of these bonds into two sets, G_I and G_R . G_I is the set of symmetries that leave the bond invariant up to a lattice translation, while G_R contains the symmetries that reverse the bond by switching the positions of the atoms in the bond, up to a lattice translation. The FCM will then satisfy the conditions

$$\Phi^{\alpha\beta}(\mathbf{R}_i - \mathbf{R}_j) = \begin{cases} S^T \Phi^{\alpha\beta}(\mathbf{R}_i - \mathbf{R}_j) S & \text{if } S \in G_I, \\ S^T \Phi^{\alpha\beta}(\mathbf{R}_i - \mathbf{R}_j)^T S & \text{if } S \in G_R. \end{cases} \quad (\text{B4})$$

Following Ref. [78], we consider connections up to the third nearest neighbors and explicitly find five distinct bonds, while the rest can be expressed in terms of these by applying Eq. (B4).

$$\begin{aligned}
\Phi^{11}((2a, 0)) : \quad & G_I = \{E, \sigma_y\}, & G_R = \{C_{2z}, \sigma_x\} & \implies \Phi^{11}((2a, 0)) = \begin{pmatrix} \eta_1^1 & 0 \\ 0 & \eta_2^1 \end{pmatrix}, \\
\Phi^{22}((2a, 0)) : \quad & G_I = \{E, \sigma_y\}, & G_R = \{C_{2z}, \sigma_x\} & \implies \Phi^{22}((2a, 0)) = \begin{pmatrix} \eta_1^2 & 0 \\ 0 & \eta_2^2 \end{pmatrix}, \\
\Phi^{33}((2a, 0)) : \quad & G_I = \{E, \sigma_y\}, & G_R = \{C_{2z}, \sigma_x\} & \implies \Phi^{33}((2a, 0)) = \begin{pmatrix} \eta_1^3 & 0 \\ 0 & \eta_2^3 \end{pmatrix}, \\
\Phi^{12}((0, 0)) : \quad & G_I = \{E, \sigma_y\}, & G_R = \emptyset & \implies \Phi^{12}((0, 0)) = \begin{pmatrix} \gamma_1 & 0 \\ 0 & \gamma_2 \end{pmatrix}, \\
\Phi^{13}((0, 0)) : \quad & G_I = \{E\}, & G_R = \{\sigma_{xy}\} & \implies \Phi^{13}((0, 0)) = \begin{pmatrix} \rho_1 & \rho_2 \\ \rho_3 & \rho_1 \end{pmatrix}.
\end{aligned}$$

This method leaves, in principle, eleven free parameters, where η is the bond strength between atoms of the same type, γ is the NN strength, and ρ is the NNN strength. To narrow down the number of free parameters, we consider the bond strength between all NN, etc., to be equal, hence $\eta_i^j = \eta$, $\gamma_i = \gamma$, and $\rho_i = \rho$. When determining the ratio of η , γ , and ρ , we assume the bond strength to decrease linearly with distance, such that $\gamma = 2\eta$ and $\rho = \sqrt{2}\eta$. With these conditions, we only have one free parameter, η . We have chosen $\eta = -1.8\text{N/m}$, so that the phonon bandwidth is about 30 meV, as illustrated in Fig. 1(b). Also, due to the condition of equal bond strength for the three basis atoms, we have set all their masses equal, $M_\alpha = 12 \text{ u} \forall \alpha$.

The rest of the FCM elements can be found by utilizing Eq. (B4), which gives

$$\begin{aligned}
\Phi^{11}((0, 2a)) &= \sigma_{xy}^T \Phi^{33}((2a, 0)) \sigma_{xy}, \\
\Phi^{11}((0, -2a)) &= \sigma_y^T \Phi^{11}((0, 2a)) \sigma_y, \\
\Phi^{11}((-2a, 0)) &= \Phi^{11}((2a, 0))^T, \\
\Phi^{22}((0, 2a)) &= C_{4z+}^T \Phi^{22}((2a, 0)) C_{4z+}, \\
\Phi^{22}((-2a, 0)) &= C_{4z+}^T \Phi^{22}((0, 2a)) C_{4z+}, \\
\Phi^{22}((0, -2a)) &= C_{4z+}^T \Phi^{22}((-2a, 0)) C_{4z+}, \\
\Phi^{33}((-2a, 0)) &= \sigma_x^T \Phi^{33}((2a, 0)) \sigma_x, \\
\Phi^{33}((0, 2a)) &= \sigma_{xy}^T \Phi^{11}((2a, 0)) \sigma_{xy}, \\
\Phi^{33}((0, -2a)) &= \Phi^{33}((0, 2a))^T, \\
\Phi^{12}((2a, 0)) &= \sigma_x^T \Phi^{12}((0, 0)) \sigma_x, \\
\Phi^{23}((0, 0)) &= C_{4z+}^T \Phi^{12}((0, 0))^T C_{4z+}, \\
\Phi^{23}((0, -2a)) &= C_{4z-}^T \Phi^{12}((0, 0))^T C_{4z-}, \\
\Phi^{13}((2a, 0)) &= \sigma_x^T \Phi^{13}((0, 0)) \sigma_x, \\
\Phi^{13}((0, -2a)) &= \sigma_y^T \Phi^{13}((0, 0)) \sigma_y.
\end{aligned}$$

$$\Phi^{13}((2a, -2a)) = \sigma_{xy}^T \Phi^{13}((0, 0))^T \sigma_{\overline{xy}}.$$

What remains to be determined are the three self-force elements, which are determined by using Eq. (B2), and are given by

$$\begin{aligned}
\Phi_{(0,0)}^{11} &= -2 \begin{pmatrix} \eta_1^1 + \eta_2^3 + \gamma_1 + 2\rho_1 & 0 \\ 0 & \eta_2^1 + \eta_1^3 + \gamma_2 + 2\rho_1 \end{pmatrix}, \\
\Phi_{(0,0)}^{22} &= -2 \begin{pmatrix} \eta_1^2 + \eta_2^2 + \gamma_1 + \gamma_2 & 0 \\ 0 & \eta_1^2 + \eta_2^2 + \gamma_1 + \gamma_2 \end{pmatrix}, \\
\Phi_{(0,0)}^{33} &= -2 \begin{pmatrix} \eta_2^1 + \eta_1^3 + \gamma_2 + 2\rho_1 & 0 \\ 0 & \eta_1^1 + \eta_2^3 + \gamma_1 + 2\rho_1 \end{pmatrix}.
\end{aligned}$$

This model can be extended to include bonds in the z -direction by adding the mirror symmetry of the z -plane, σ_z , in all G_I sets, which will leave an additional independent parameter [78]. However, as we will see in Sec. C, the electron-phonon interaction with oscillations in the z -direction will be of higher order in the displacements, so we neglect these phonon modes. To solve for the phonon modes and frequencies, we turn to momentum-space, where the dynamical matrix is the Fourier transformation of the FCM, $D_{\mu\nu}^{\alpha\beta}(\mathbf{k}) \equiv \sum_i \Phi_{\mu\nu}^{\alpha\beta}(\mathbf{R}_i - \mathbf{R}_j) e^{-i\mathbf{k} \cdot (\mathbf{R}_{i\alpha} - \mathbf{R}_{j\beta})}$, which will then be a 6×6 matrix with elements

$$D(\mathbf{k}) = \begin{pmatrix} D^{11}(\mathbf{k}) & D^{12}(\mathbf{k}) & D^{13}(\mathbf{k}) \\ D^{12}(\mathbf{k})^\dagger & D^{22}(\mathbf{k}) & D^{23}(\mathbf{k}) \\ D^{13}(\mathbf{k})^\dagger & D^{23}(\mathbf{k})^\dagger & D^{33}(\mathbf{k}) \end{pmatrix},$$

$$D_{xx}^{11}(\mathbf{k}) = 2 [\eta_1^1 (\cos(2k_x a) - 1) + \eta_2^3 (\cos(2k_y a) - 1) - \gamma_1 - 2\rho_1],$$

$$D_{yy}^{11}(\mathbf{k}) = 2 [\eta_2^1 (\cos(2k_x a) - 1) + \eta_1^3 (\cos(2k_y a) - 1) - \gamma_2 - 2\rho_1],$$

$$D_{xx}^{22}(\mathbf{k}) = 2 [\eta_1^2 (\cos(2k_x a) - 1) + \eta_2^2 (\cos(2k_y a) - 1) - \gamma_1 - \gamma_2],$$

$$D_{yy}^{22}(\mathbf{k}) = 2 [\eta_2^2 (\cos(2k_x a) - 1) + \eta_1^2 (\cos(2k_y a) - 1) - \gamma_1 - \gamma_2],$$

$$D_{xx}^{33}(\mathbf{k}) = 2 [\eta_1^3 (\cos(2k_x a) - 1)$$

$$\begin{aligned}
& +\eta_2^1 (\cos(2k_y a) - 1) - \gamma_2 - 2\rho_1], \\
D_{yy}^{33}(\mathbf{k}) &= 2 [\eta_2^3 (\cos(2k_x a) - 1) \\
& +\eta_1^1 (\cos(2k_y a) - 1) - \gamma_1 - 2\rho_1], \\
D_{xx}^{12}(\mathbf{k}) &= 2\gamma_1 \cos(k_x a), \\
D_{yy}^{12}(\mathbf{k}) &= 2\gamma_2 \cos(k_x a), \\
D_{xx}^{13}(\mathbf{k}) &= 4\rho_1 \cos(k_x a) \cos(k_y a), \\
D_{xy}^{13}(\mathbf{k}) &= 4\rho_2 \sin(k_x a) \sin(k_y a), \\
D_{yx}^{13}(\mathbf{k}) &= 4\rho_3 \sin(k_x a) \sin(k_y a), \\
D_{yy}^{13}(\mathbf{k}) &= 4\rho_1 \cos(k_x a) \cos(k_y a), \\
D_{xx}^{23}(\mathbf{k}) &= 2\gamma_2 \cos(k_y a), \\
D_{yy}^{23}(\mathbf{k}) &= 2\gamma_1 \cos(k_y a).
\end{aligned}$$

The dynamical matrix is Hermitian, so the elements that are not listed above and cannot be found by the constraint of hermiticity are zero. The eigenvalue problem for the dynamical matrix is given by Eq. (1).

Appendix C: Electron-phonon coupling

Similar to Ref. [79], we model the electron-phonon interaction by expanding the hopping parameters t and t_2 around the equilibrium position of the lattice. We assume the atomic orbitals to be Gaussian,

$$\begin{aligned}
\phi_{\mathbf{r}_{i\alpha}}(\mathbf{r}) &= \frac{1}{\pi^{3/4} \sqrt{\sigma_x \sigma_y \sigma_z}} \\
&\times \exp\left(-\frac{(x - r_{i\alpha}^x)^2}{2\sigma_x^2} - \frac{(y - r_{i\alpha}^y)^2}{2\sigma_y^2} - \frac{(z - r_{i\alpha}^z)^2}{2\sigma_z^2}\right), \quad (\text{C1})
\end{aligned}$$

where $\mathbf{r}_{i\alpha}$ denote the instantaneous position of atom α in unit cell i , \mathbf{r} is the spatial coordinate of the wavefunction, σ_x , σ_y , and σ_z are standard deviations in the three spatial directions. The hopping amplitudes are given by the overlap between two different atomic orbitals modulated by the crystal potential [86]²

$$\begin{aligned}
t(\mathbf{r}_{i\alpha} - \mathbf{r}_{j\beta}) &= \int d^3r \phi_{\mathbf{r}_{i\alpha}}(\mathbf{r}) A(\mathbf{r}) \phi_{\mathbf{r}_{j\beta}}(\mathbf{r}) \\
&= A \exp\left(-\frac{r_{ij\alpha\beta}^x{}^2}{4\sigma_x^2} - \frac{r_{ij\alpha\beta}^y{}^2}{4\sigma_y^2} - \frac{r_{ij\alpha\beta}^z{}^2}{4\sigma_z^2}\right), \quad (\text{C2})
\end{aligned}$$

where $\mathbf{r}_{i\alpha j\beta} \equiv \mathbf{r}_{i\alpha} - \mathbf{r}_{j\beta}$, and $A(\mathbf{r})$ depends on the crystal potential, which we assume to be constant in space. We choose A such that $t = 2.4$ eV for $\sigma_x = \sigma_y = \sigma_z = 0.4a$. Note that when we consider non-zero t_2 , it is found from the above equation with the same A , giving $t_2 \approx 0.21t$, while we also consider $t_2 = 0$ by artificially setting it to zero.

We Taylor expand the hopping amplitude to first order in displacements from equilibrium, \mathbf{u} , as $t(\mathbf{r}_{ij\alpha\beta}) \approx t(\mathbf{R}_{ij\alpha\beta}) + \mathbf{u}_{ij\alpha\beta} \cdot \nabla t$, where we defined the short-hand notation $\nabla t \equiv \nabla_{\mathbf{r}} t(\mathbf{r}_{ij\alpha\beta}) \Big|_{\mathbf{r}_{ij\alpha\beta} = \mathbf{R}_{ij\alpha\beta}}$. The gradient of the hopping is given by

$$\begin{aligned}
\nabla_{\mathbf{r}} t(\mathbf{r}_{ij\alpha\beta}) &= -A \exp\left(-\frac{r_{ij\alpha\beta}^x{}^2}{4\sigma_x^2} - \frac{r_{ij\alpha\beta}^y{}^2}{4\sigma_y^2} - \frac{r_{ij\alpha\beta}^z{}^2}{4\sigma_z^2}\right) \\
&\times \left(\frac{r_{ij\alpha\beta}^x}{2\sigma_x^2}, \frac{r_{ij\alpha\beta}^y}{2\sigma_y^2}, \frac{r_{ij\alpha\beta}^z}{4\sigma_z^2}\right), \quad (\text{C3})
\end{aligned}$$

where we note that at equilibrium, the z -component is zero. Such that to first order of the displacements, the electrons do not couple to the OOP phonon modes. We find the electron-phonon interaction by inserting this expansion in the electron Hamiltonian in Eq. (2). The first term in the expansion will simply give the electron hopping term, while the electron-phonon Hamiltonian is then given by

$$H_{\text{el-ph}} = \sum_{(i,j)\sigma\alpha\beta} (\mathbf{u}_{i\alpha} - \mathbf{u}_{j\beta}) \cdot \nabla t c_{i\alpha\sigma}^\dagger c_{j\beta\sigma}, \quad (\text{C4})$$

which, after inserting the Fourier transformed operators, quantifying the displacements, and utilizing the electron band operators as described in Sec. IV, can be written as

$$H_{\text{el-ph}} = \sum_{\mathbf{k}\mathbf{q}\sigma\lambda} g_{\sigma\lambda}^{(1)}(\mathbf{k}, \mathbf{k} + \mathbf{q}) (a_{-\mathbf{q},\lambda}^\dagger + a_{\mathbf{q}\lambda}) d_{\mathbf{k}+\mathbf{q},\sigma}^\dagger d_{\mathbf{k}\sigma}, \quad (\text{C5})$$

where we have omitted the band index, as we only consider scattering on the Fermi surface (FS). The electron-phonon coupling is given by

$$\begin{aligned}
g_{\sigma\lambda}^{(1)}(\mathbf{k}, \mathbf{k} + \mathbf{q}) &= \frac{t}{2} \sqrt{\frac{\hbar}{2N\omega_{\mathbf{q}\lambda}}} \sum_{\alpha\beta} q_{\mathbf{k}+\mathbf{q},\sigma\alpha}^* q_{\mathbf{k}\sigma\beta} \\
&\times \sum_{\delta} e^{i\mathbf{k}\cdot\delta} \left(\frac{\delta_x}{\sigma_x^2}, \frac{\delta_y}{\sigma_y^2}\right) \cdot \left[\frac{\hat{\mathbf{e}}_{\mathbf{q}\lambda}^\alpha}{\sqrt{M_\beta}} e^{i\mathbf{q}\cdot\delta} - \frac{\hat{\mathbf{e}}_{\mathbf{q}\lambda}^\alpha}{\sqrt{M_\alpha}}\right], \quad (\text{C6})
\end{aligned}$$

where δ are the equilibrium NN vectors. The same procedure can be done for the NNN hopping t_2 , which gives an electron-phonon coupling $g_{\sigma\lambda}^{(2)}(\mathbf{k}, \mathbf{k} + \mathbf{q})$, that is almost identical to Eq. (C6), only differing with the substitutions $t \rightarrow t_2$ and $\delta \rightarrow \delta_2$, where δ_2 are the vectors between NNNs at equilibrium. The total electron-phonon coupling is then given by $g_{\sigma\lambda}(\mathbf{k}, \mathbf{k} + \mathbf{q}) \equiv g_{\sigma\lambda}^{(1)}(\mathbf{k}, \mathbf{k} + \mathbf{q}) + g_{\sigma\lambda}^{(2)}(\mathbf{k}, \mathbf{k} + \mathbf{q})$.

1. Effective electron-electron interaction

The electron-phonon interaction can be written as an effective electron-electron interaction by applying a Schrieffer-Wolff transformation [81]. Let the full Hamiltonian be given by $H = H_0 + \zeta H_1$, where $H_0 = H_{\text{el}} + H_{\text{ph}}$, $H_1 = H_{\text{el-ph}}$, and ζ is a smallness parameter for the perturbation. We apply

² We assume the atomic orbitals are eigenstates of the kinetic term and the on-site part of the crystal potential.

a unitary transformation to the full Hamiltonian as

$$\begin{aligned} H' &= e^{-\zeta S} H e^{\zeta S} \\ &= H_0 + \zeta (H_1 + [H_0, S]) \\ &\quad + \zeta^2 [H_1, S] + \frac{1}{2} \zeta^2 [[H_0, S], S] + \mathcal{O}(\zeta^3). \end{aligned} \quad (\text{C7})$$

The terms in linear order of ζ vanish if we choose S such that

$$H_1 + [H_0, S] = 0, \quad (\text{C8})$$

which leaves the transformed Hamiltonian to be

$$H' = H_0 + \frac{1}{2} \zeta^2 [H_1, S] + \mathcal{O}(\zeta^3). \quad (\text{C9})$$

To find the S satisfying Eq. (C8), we start by looking at H_0 and H_1 ,

$$H_0 = \sum_{\mathbf{k}\sigma} \varepsilon_{\mathbf{k}\sigma} d_{\mathbf{k}\sigma}^\dagger d_{\mathbf{k}\sigma} + \sum_{\mathbf{q}\lambda} \hbar\omega_{\mathbf{q}\lambda} \left(a_{\mathbf{q}\lambda}^\dagger a_{\mathbf{q}\lambda} + \frac{1}{2} \right), \quad (\text{C10})$$

$$H_1 = \sum_{\mathbf{k}\mathbf{q}\sigma\lambda} g_{\lambda\sigma}(\mathbf{k}, \mathbf{k} + \mathbf{q}) \left(a_{-\mathbf{q},\lambda}^\dagger + a_{\mathbf{q}\lambda} \right) d_{\mathbf{k}+\mathbf{q},\sigma}^\dagger d_{\mathbf{k}\sigma}. \quad (\text{C11})$$

From these expressions, we make an ansatz for S as

$$\begin{aligned} S &= \sum_{\mathbf{k}\mathbf{q}\sigma\lambda} g_{\lambda\sigma}(\mathbf{k}, \mathbf{k} + \mathbf{q}) \\ &\quad \times \left(x_{\mathbf{k}\mathbf{q}\sigma\lambda} a_{-\mathbf{q},\lambda}^\dagger + y_{\mathbf{k}\mathbf{q}\sigma\lambda} a_{\mathbf{q}\lambda} \right) d_{\mathbf{k}+\mathbf{q},\sigma}^\dagger d_{\mathbf{k}\sigma}, \end{aligned} \quad (\text{C12})$$

solving for the coefficients $x_{\mathbf{k}\mathbf{q}\sigma\lambda}$ and $y_{\mathbf{k}\mathbf{q}\sigma\lambda}$ by applying the condition Eq. (C8) gives

$$x_{\mathbf{k}\mathbf{q}\sigma\lambda} = \frac{1}{\varepsilon_{\mathbf{k}\sigma} - \varepsilon_{\mathbf{k}+\mathbf{q},\sigma} - \hbar\omega_{\mathbf{q}\lambda}}, \quad (\text{C13})$$

$$y_{\mathbf{k}\mathbf{q}\sigma\lambda} = \frac{1}{\varepsilon_{\mathbf{k}\sigma} - \varepsilon_{\mathbf{k}+\mathbf{q},\sigma} + \hbar\omega_{\mathbf{q}\lambda}}. \quad (\text{C14})$$

Note that since we have assumed the scattering to be contained on the FS, the two electron energies in the denominators will cancel. We can now find the effective electron-electron interaction in Eq. (C9), where we only keep terms corresponding to electron-electron interactions and neglect higher-order phonon terms,

$$\begin{aligned} H_{\text{eff}} &= \frac{1}{2} \sum_{\mathbf{k}\mathbf{q}\sigma} \sum_{\lambda\mathbf{k}'\sigma'} g_{\lambda\sigma}(\mathbf{k}, \mathbf{k} + \mathbf{q}) g_{\lambda\sigma'}(\mathbf{k}', \mathbf{k}' - \mathbf{q}) \\ &\quad \times (y_{\mathbf{k}\mathbf{q}\sigma\lambda} - x_{\mathbf{k}\mathbf{q}\sigma\lambda}) d_{\mathbf{k}+\mathbf{q},\sigma}^\dagger d_{\mathbf{k}'-\mathbf{q},\sigma'}^\dagger d_{\mathbf{k}\sigma} d_{\mathbf{k}'\sigma'}. \end{aligned} \quad (\text{C15})$$

As explained in Sec. V, we consider spin-polarized, zero-momentum Cooper pairs, which set the conditions $\sigma' = \sigma$ and $\mathbf{k}' = -\mathbf{k}$. With these assumptions, the interaction takes the form

$$H_{\text{eff}} = \sum_{\mathbf{k}\mathbf{k}'\sigma} V_{\mathbf{k}'\mathbf{k}\sigma} d_{\mathbf{k}'\sigma}^\dagger d_{-\mathbf{k}',\sigma}^\dagger d_{-\mathbf{k},\sigma} d_{\mathbf{k}\sigma}, \quad (\text{C16})$$

where we defined a new summation variable $\mathbf{k}' \equiv \mathbf{k} + \mathbf{q}$, and the interaction strength is given by

$$V_{\mathbf{k}'\mathbf{k}\sigma} = - \sum_{\lambda} \frac{g_{\sigma\lambda}(\mathbf{k}, \mathbf{k}') g_{\sigma\lambda}(-\mathbf{k}, -\mathbf{k}')}{\hbar\omega_{\mathbf{k}'-\mathbf{k},\lambda}}, \quad (\text{C17})$$

with the momenta on the FS of spin σ . We follow the procedure of Ref. [58] and symmetrize the interaction, giving the effective electron-electron Hamiltonian

$$\begin{aligned} H_{\text{eff}} &= \frac{1}{2} \sum_{\mathbf{k}\mathbf{k}'\sigma} \bar{V}_{\mathbf{k}'\mathbf{k}\sigma} d_{\mathbf{k}'\sigma}^\dagger d_{-\mathbf{k}',\sigma}^\dagger d_{-\mathbf{k},\sigma} d_{\mathbf{k}\sigma}, \\ 2\bar{V}_{\mathbf{k}'\mathbf{k}\sigma} &= V_{\mathbf{k}'\mathbf{k}\sigma} + V_{-\mathbf{k}',-\mathbf{k},\sigma} - V_{-\mathbf{k},\mathbf{k}\sigma} - V_{\mathbf{k}',-\mathbf{k},\sigma}. \end{aligned} \quad (\text{C18})$$

Appendix D: Details of the effective interaction on the Fermi surface

In this section, we discuss in more detail the momentum dependence of the effective electron-electron interaction on the FS. We introduce the quantity $\Lambda_{k_{\parallel} k'_{\parallel} \sigma}$ via the linearized Fermi-surface averaged gap equation [39, 58, 83]

$$\begin{aligned} \lambda \Delta_{k_{\parallel} \sigma} &= - \frac{N S_{\text{FS}}}{A_{\text{BZ}} N_{\text{samp}}} \sum_{k'_{\parallel}} \left| \frac{d\varepsilon}{dk'_{\perp}} \right|^{-1} \bar{V}_{k_{\parallel} k'_{\parallel} \sigma} \Delta_{k'_{\parallel} \sigma} \\ &\equiv \sum_{k'_{\parallel}} \Lambda_{k_{\parallel} k'_{\parallel} \sigma} \Delta_{k'_{\parallel} \sigma}, \end{aligned} \quad (\text{D1})$$

where the meaning of the symbols is explained under Eq. (9). This constitutes an eigenvalue problem for a positive quantity λ with eigenvector $\Delta_{k_{\parallel} \sigma}$, and it is the momentum structure of the matrix $\Lambda_{k_{\parallel} k'_{\parallel} \sigma}$ that determines whether or not non-trivial solutions exist. Some of these matrix elements are plotted on the FS in Fig. 5 (left and middle column), along with the eigenvectors $\Delta_{k_{\parallel} \sigma}$ on the FS in the right column. Notice how both the symmetrized interaction $\bar{V}_{\mathbf{k}\mathbf{k}'\sigma}$ as well as the density of states factor $\left| \frac{d\varepsilon}{dk'_{\perp}} \right|^{-1}$ enters in $\Lambda_{k_{\parallel} k'_{\parallel} \sigma}$. In the first row of Fig. 5 with $t_2 = 0$ and $\mu = 0.1t$, Fig. 4(a), shows that the dimensionless coupling is $\lambda_m \approx 0.01$, which is too low to give a non-negligible T_c . From Eq. (D1) and Fig. 5 (a), we see that $\Lambda_{k_{\parallel} k'_{\parallel} \downarrow}$ has a disadvantageous sign, as discussed in Sec. V. It is also most substantial for $\mathbf{k}' = \pm\mathbf{k}$ along the $\Gamma\mathbf{X}$ line. Hence, it is natural that the eigenvector with the largest eigenvalue has zero gap on the $\Gamma\mathbf{X}$ line. Figure 5(b) shows $\Lambda_{k_{\parallel} k'_{\parallel} \downarrow}$ when \mathbf{k} is placed at the maximal gap amplitude. For that value of \mathbf{k} , we see that $|\Lambda_{k_{\parallel} k'_{\parallel} \downarrow}|$ is not maximal at $\mathbf{k}' = \pm\mathbf{k}$, rather it is maximal for \mathbf{k}' on the $\Gamma\mathbf{X}$ line.

By comparing the coupling in Fig. 5 (b) with the gap in Fig. 5 (c), we see how appropriate sign changes of the gap generate an eigenvector with a positive eigenvalue λ_m . From Fig. 5 (b), we see that $|\Lambda_{k_{\parallel} k'_{\parallel} \downarrow}|$ with \mathbf{k} placed in the maximum positive gap ($\Delta_{\mathbf{k}\downarrow} > 0$) and \mathbf{k}' placed in the maximum negative gap ($\Delta_{\mathbf{k}'\downarrow} < 0$, $\mathbf{k}' = \mathbf{N}$), is smaller than the maximum $|\Lambda_{k_{\parallel} k'_{\parallel} \downarrow}|$ in Fig. 5 (a). As a result, the eigenvector is barely able to satisfy the requirement of positive eigenvalue, and λ_m is small.

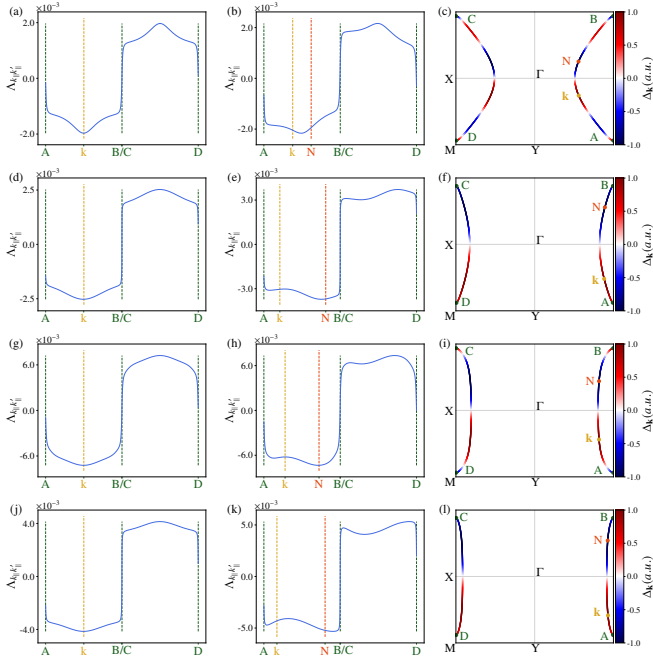


FIG. 5. The first column shows the matrix elements $\Lambda_{k_{\parallel}k'_{\parallel}\sigma}$ for spin-down, with \mathbf{k} given by the yellow dashed line, corresponding to the midpoint between A and B in the respective plot in the third column, and \mathbf{k}' is given by the position along the path. The second column has \mathbf{k} as marked in the respective third column plots, corresponding to the maximum of the gap. The third column shows the gap for spin-down. The rows are structured such that in the first row (a-c), we have used ($t_2 = 0, \mu = 0.1t$), in the second (d-f) ($t_2 = 0, \mu = 0.25t$), in the third (g-i) ($t_2 \approx 0.21t, \mu = 0.1t$), and in the fourth (j-l) ($t_2 \approx 0.21t, \mu = 0.25t$). N indicates the momentum with the most negative value for the gap. Table I lists the remaining parameters.

Then, in the second row of Fig. 5 with $t_2 = 0$ and $\mu = 0.25t$, Fig. 4(a) shows that $\lambda_m \approx 0.20$, which is larger than the first row by a considerable amount, leading to a non-vanishing critical temperature. This may be understood from the fact that the maximal magnitude of $|\Lambda_{k_{\parallel}k'_{\parallel}\downarrow}|$ is much greater in Fig. 5 (e) than in Fig. 5 (d). Also, unlike the first row [Fig. 5 (b)], the peak of $|\Lambda_{k_{\parallel}k'_{\parallel}\downarrow}|$ in Fig. 5 (e) occurs close to where \mathbf{k} is placed in the maximum positive gap and \mathbf{k}' is placed in the maximum negative gap. Hence, the sign change of the gap function takes significant advantage of the coupling, giving a greater eigenvalue λ_m .

The situation in the third and fourth rows with $t_2 \approx 0.21t$, is very similar to the second row. In the third row, however, the difference in magnitudes $|\Lambda_{k_{\parallel}k'_{\parallel}\downarrow}|$ between column one and two is about the same as in the first row, but an important difference is that the values of $|\Lambda_{k_{\parallel}k'_{\parallel}\downarrow}|$ are larger, making it possible to have a higher λ_m . More importantly, the shape of $\Lambda_{k_{\parallel}k'_{\parallel}\downarrow}$ in Fig. 5 (h) is more similar to Figs. 5 (e) and 5 (k) than Fig. 5 (b). This gives a markedly different momentum structure of the gap in rows two, three, and four [Figs. 5 (f), 5 (i), and 5 (l)] compared to row one [Fig. 5 (c)]. This difference in

the momentum dependence of the coupling and gap function enables a larger eigenvalue λ_m .

The increased λ_m when including NNN hopping is understood from the effect of non-zero t_2 on the inverse slope of the FS, shown in Fig. 2 (b). Compared to $t_2 = 0$, the slope is not as strongly peaked along the ΓX line, reducing the adverse effects of $|\Lambda_{k_{\parallel}k'_{\parallel}\downarrow}|$ with $\mathbf{k}' = \pm\mathbf{k}$ on the ΓX line. As mentioned in Sec. V, a non-zero t_2 also enables more electron-phonon processes, which increases the coupling strength.

Appendix E: Finite-momentum Cooper pairs

In the Sec. V, we have focused on spin-polarized pairing. However, there is still a possibility for both singlet and spin-zero triplet states. To form different-spin Cooper pairs, a finite-momentum state is required, effectively shifting one of the spin-FS in Fig. 2(a) on top of the other, as illustrated in Fig. 6. Even in the case of maximum overlap, there is a significantly smaller area as opposed to the spin-polarized case, where the whole region between the solid lines can form Cooper pairs. In the cases of Fig. 6 (a) and (b), where we have maximized the overlap, the intersection area is 0.073 times the area of the

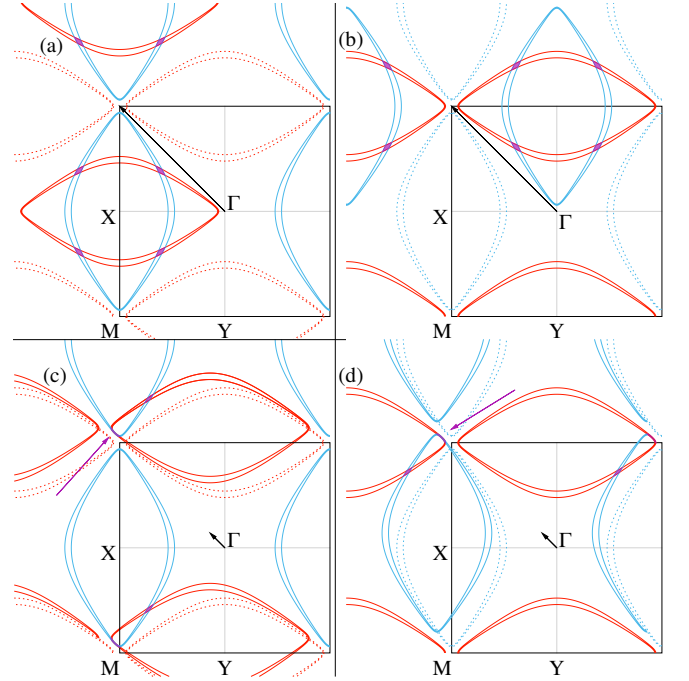


FIG. 6. The box marks the BZ, solid lines denote states with energies within a phonon bandwidth of the Fermi level, and the dashed lines indicate which FS is shifted. The overlap between the shifted FS and the opposite spin-FS is marked in purple. The spin-up FS is shifted in (a) and (c), while for (b) and (d), it is spin-down. The vector starting in the Γ -point is the finite-momentum vector, showing how the FS is shifted. The finite-momentum vector is chosen to maximize the overlap in (a) and (b), while for (c) and (d), it sets the overlap at the ends of the ellipses highlighted by the purple arrow. In all the cases, $\mu = 0.1$ and $t_2 = 0$, as these values give relatively large overlap. See Table I for the remaining parameters.

spin-polarized case. While for the case of Fig. 6 (c) and (d), the intersection area is 0.016 times the spin-polarized area. Let us compare this to Fig. 1(b) in Ref. [54]. In their model, the ellipses have a rather large overlap for the case comparable to our Fig. 6 (c) and (d). The Lieb lattice model has much sharper edges of the ellipses here, and much more dispersive bands in this region compared to the rest of the ellipse, both of which significantly reduces the likelihood of finite-momentum pairing compared to the model of Ref. [54] and other models that have studied the competition of zero-momentum and finite-momentum pairing in altermagnets [55]. Also note that the case in Fig. 6 (a) and (b) is comparable to Fig. 1(a) in Ref. [54] with 4 discrete overlap points of the FSs, only that in our case it also requires finite momentum since the spin up and spin down FSs have no overlap originally. Such a state is not expected to be competitive at strong spin splitting [54], which is the case we focus on.

Appendix F: Numerical parameters

Table I shows the value of parameters that are the same throughout the paper. Parameters varied are given in the caption of their respective figures. The number of sampling points varies with the FS length. We have a uniform spacing of $6 \times 10^{-3}/a$ between neighboring points. The value in Tab. I is a typical number.

TABLE I. List of parameters

Parameter	Value
a	1 Å
σ_x	0.4a
σ_y	0.4a
t	2.4 eV
$J_{sd}S$	0.7 eV
η	-1.8 N/m
ρ	$\sqrt{2}\eta$
γ	2 η
M_α	12 u
N_{samp}	800

-
- [1] H. K. Onnes, Further experiments with liquid helium, Commun. Phys. Lab. Univ. Leiden 120b, 122b, 124c (1911), reprinted in Proc. K. Ned. Akad. Wet. **13**, 1274 (1911), *ibid.* **14**, 113 (1911), *ibid.* **14**, 818 (1911).
- [2] D. van Delft and P. Kes, The discovery of superconductivity, *Phys. Today* **63**, 38 (2010).
- [3] P. W. Anderson, Plasmons, gauge invariance, and mass, *Phys. Rev.* **130**, 439 (1963).
- [4] F. Englert and R. Brout, Broken symmetry and the mass of gauge vector mesons, *Phys. Rev. Lett.* **13**, 321 (1964).
- [5] P. W. Higgs, Broken symmetries and the masses of gauge bosons, *Phys. Rev. Lett.* **13**, 508 (1964).
- [6] G. S. Guralnik, C. R. Hagen, and T. W. B. Kibble, Global conservation laws and massless particles, *Phys. Rev. Lett.* **13**, 585 (1964).
- [7] W. Meissner and R. Ochsenfeld, Ein neuer Effekt bei Eintritt der Supraleitfähigkeit, *Naturwissenschaften* **21**, 787 (1933).
- [8] J. Bardeen, L. N. Cooper, and J. R. Schrieffer, Theory of Superconductivity, *Phys. Rev.* **108**, 1175 (1957).
- [9] F. Steglich, J. Aarts, C. D. Bredl, W. Lieke, D. Meschede, W. Franz, and H. Schäfer, Superconductivity in the Presence of Strong Pauli Paramagnetism: CeCu₂Si₂, *Phys. Rev. Lett.* **43**, 1892 (1979).
- [10] B. White, J. Thompson, and M. Maple, Unconventional superconductivity in heavy-fermion compounds, *Physica C: Superconductivity and its Applications* **514**, 246 (2015), superconducting Materials: Conventional, Unconventional and Undetermined.
- [11] G. Bednorz and K. A. Mueller, Possible high t_c superconductivity in the ba-la-cu-o system, *Z. Physik B* **64**, 189 (1986).
- [12] P. Monthoux and D. Pines, YBa₂Cu₃O₇: A nearly antiferromagnetic Fermi liquid, *Phys. Rev. B* **47**, 6069 (1993).
- [13] D. J. Scalapino, Superconductivity and Spin Fluctuations, *J. Low Temp. Phys.* **117**, 179 (1999).
- [14] T. Moriya and K. Ueda, Antiferromagnetic spin fluctuation and superconductivity, *Rep. Prog. Phys.* **66**, 1299 (2003).
- [15] P. J. Hirschfeld, M. M. Korshunov, and I. I. Mazin, Gap symmetry and structure of Fe-based superconductors, *Rep. Prog. Phys.* **74**, 124508 (2011).
- [16] M. Sigrist and K. Ueda, Phenomenological theory of unconventional superconductivity, *Rev. Mod. Phys.* **63**, 239 (1991).
- [17] D. A. Wollman, D. J. Van Harlingen, W. C. Lee, D. M. Ginsberg, and A. J. Leggett, Experimental determination of the superconducting pairing state in YBCO from the phase coherence of YBCO-Pb dc SQUIDS, *Phys. Rev. Lett.* **71**, 2134 (1993).
- [18] V. L. Ginzburg, Ferromagnetic superconductors, *Zh. Eksp. Teor. Fiz.* **31**, 202 (1956), [*Sov. Phys. JETP*, **4**, 153 (1957)].
- [19] D. Fay and J. Appel, Coexistence of p -state superconductivity and itinerant ferromagnetism, *Phys. Rev. B* **22**, 3173 (1980).
- [20] X. Jian, J. Zhang, Q. Gu, and R. A. Klemm, Enhancement of ferromagnetism by p -wave Cooper pairing in superconducting ferromagnets, *Phys. Rev. B* **80**, 224514 (2009).
- [21] S. S. Saxena, P. Agarwal, K. Ahilan, F. M. Grosche, R. K. W. Haselwimmer, M. J. Steiner, E. Pugh, I. R. Walker, S. R. Julian, P. Monthoux, G. G. Lonzarich, A. Huxley, I. Sheikin, D. Braithwaite, and J. Flouquet, Superconductivity on the border of itinerant-electron ferromagnetism in UGe₂, *Nature* **406**, 587 (2000).
- [22] N. T. Huy, A. Gasparini, D. E. de Nijs, Y. Huang, J. C. P. Klaasse, T. Gortenmulder, A. de Visser, A. Hamann, T. Görlach, and H. v. Löhneysen, Superconductivity on the Border of Weak Itinerant Ferromagnetism in UCoGe, *Phys. Rev. Lett.* **99**, 067006 (2007).
- [23] M. Kargarian, D. K. Efimkin, and V. Galitski, Amperean Pairing at the Surface of Topological Insulators, *Phys. Rev. Lett.* **117**, 076806 (2016).
- [24] H. G. Hugdal, S. Rex, F. S. Nogueira, and A. Sudbø, Magnon-induced superconductivity in a topological insulator coupled to

- ferromagnetic and antiferromagnetic insulators, *Phys. Rev. B* **97**, 195438 (2018).
- [25] N. Rohling, E. L. Fjærbu, and A. Brataas, Superconductivity induced by interfacial coupling to magnons, *Phys. Rev. B* **97**, 115401 (2018).
- [26] E. L. Fjærbu, N. Rohling, and A. Brataas, Superconductivity at metal-antiferromagnetic insulator interfaces, *Phys. Rev. B* **100**, 125432 (2019).
- [27] E. Erlandsen, A. Kamra, A. Brataas, and A. Sudbø, Enhancement of superconductivity mediated by antiferromagnetic squeezed magnons, *Phys. Rev. B* **100**, 100503 (2019).
- [28] E. Thingstad, E. Erlandsen, and A. Sudbø, Eliashberg study of superconductivity induced by interfacial coupling to antiferromagnets, *Phys. Rev. B* **104**, 014508 (2021).
- [29] C. Sun, K. Mæland, and A. Sudbø, Stability of superconducting gap symmetries arising from antiferromagnetic magnons, *Phys. Rev. B* **108**, 054520 (2023).
- [30] C. Sun, K. Mæland, E. Thingstad, and A. Sudbø, Strong-coupling approach to temperature dependence of competing orders of superconductivity: Possible time-reversal symmetry breaking and nontrivial topology, *Phys. Rev. B* **109**, 174520 (2024).
- [31] H. G. Hugdal and A. Sudbø, Possible odd-frequency Amperean magnon-mediated superconductivity in topological insulator-ferromagnetic insulator bilayer, *Phys. Rev. B* **102**, 125429 (2020).
- [32] E. Erlandsen, A. Brataas, and A. Sudbø, Magnon-mediated superconductivity on the surface of a topological insulator, *Phys. Rev. B* **101**, 094503 (2020).
- [33] B. Brekke, A. Sudbø, and A. Brataas, Interfacial magnon-mediated superconductivity in twisted bilayer graphene, *New J. Phys.* **26**, 033014 (2024).
- [34] K. Mæland and A. Sudbø, Topological Superconductivity Mediated by Skyrmionic Magnons, *Phys. Rev. Lett.* **130**, 156002 (2023).
- [35] K. Mæland, S. Abnar, J. Benestad, and A. Sudbø, Topological superconductivity mediated by magnons of helical magnetic states, *Phys. Rev. B* **108**, 224515 (2023).
- [36] F. Viñas Boström and E. Viñas Boström, Magnon-mediated topological superconductivity in a quantum wire, *Phys. Rev. Res.* **6**, L022042 (2024).
- [37] E. Thingstad, J. Hutchinson, D. Loss, and J. Klinovaja, Topological Interlayer Superconductivity in a van der Waals Heterostructure, [arXiv:2405.07927](https://arxiv.org/abs/2405.07927) (2024).
- [38] L. Šmejkal, J. Sinova, and T. Jungwirth, Beyond conventional ferromagnetism and antiferromagnetism: A phase with nonrelativistic spin and crystal rotation symmetry, *Phys. Rev. X* **12**, 031042 (2022).
- [39] B. Brekke, A. Brataas, and A. Sudbø, Two-dimensional altermagnets: Superconductivity in a minimal microscopic model, *Phys. Rev. B* **108**, 224421 (2023).
- [40] M. Roig, A. Kreisel, Y. Yu, B. M. Andersen, and D. F. Agterberg, Minimal models for altermagnetism, *Phys. Rev. B* **110**, 144412 (2024).
- [41] T. Osumi, S. Souma, T. Aoyama, K. Yamauchi, A. Honma, K. Nakayama, T. Takahashi, K. Ohgushi, and T. Sato, Observation of a giant band splitting in altermagnetic MnTe, *Phys. Rev. B* **109**, 115102 (2024).
- [42] S. Lee, S. Lee, S. Jung, J. Jung, D. Kim, Y. Lee, B. Seok, J. Kim, B. G. Park, L. Šmejkal, C.-J. Kang, and C. Kim, Broken Kramers Degeneracy in Altermagnetic MnTe, *Phys. Rev. Lett.* **132**, 036702 (2024).
- [43] J. Krempaský, L. Šmejkal, S. W. D'Souza, M. Hajlaoui, G. Springholz, K. Uhlířová, F. Alarab, P. C. Constantinou, V. Strocov, D. Usanov, W. R. Pudelko, R. González-Hernández, A. Birk Hellenes, Z. Jansa, H. Reichlová, Z. Šobáň, R. D. Gonzalez Betancourt, P. Wadley, J. Sinova, D. Kriegner, J. Minár, J. H. Dil, and T. Jungwirth, Altermagnetic lifting of Kramers spin degeneracy, *Nature* **626**, 517 (2024).
- [44] S. Reimers, L. Odenbreit, L. Šmejkal, V. N. Strocov, P. Constantinou, A. B. Hellenes, R. Jaeschke Ubierno, W. H. Campos, V. K. Bharadwaj, A. Chakraborty, T. Denneulin, W. Shi, R. E. Dunin-Borkowski, S. Das, M. Kläui, J. Sinova, and M. Jourdan, Direct observation of altermagnetic band splitting in CrSb thin films, *Nat. Commun.* **15**, 2116 (2024).
- [45] J. Ding, Z. Jiang, X. Chen, Z. Tao, Z. Liu, T. Li, J. Liu, J. Sun, J. Cheng, J. Liu, Y. Yang, R. Zhang, L. Deng, W. Jing, Y. Huang, Y. Shi, M. Ye, S. Qiao, Y. Wang, Y. Guo, D. Feng, and D. Shen, Large Band Splitting in g -Wave Altermagnet CrSb, *Phys. Rev. Lett.* **133**, 206401 (2024).
- [46] F. Zhang, X. Cheng, Z. Yin, C. Liu, L. Deng, Y. Qiao, Z. Shi, S. Zhang, J. Lin, Z. Liu, M. Ye, Y. Huang, X. Meng, C. Zhang, T. Okuda, K. Shimada, S. Cui, Y. Zhao, G.-H. Cao, S. Qiao, J. Liu, and C. Chen, Crystal-symmetry-paired spin-valley locking in a layered room-temperature metallic altermagnet candidate, *Nat. Phys.* **21**, 760 (2025).
- [47] B. Jiang, M. Hu, J. Bai, Z. Song, C. Mu, G. Qu, W. Li, W. Zhu, H. Pi, Z. Wei, Y.-J. Sun, Y. Huang, X. Zheng, Y. Peng, L. He, S. Li, J. Luo, Z. Li, G. Chen, H. Li, H. Weng, and T. Qian, A metallic room-temperature d-wave altermagnet, *Nat. Phys.* **21**, 754 (2025).
- [48] C.-C. Wei, X. Li, S. Hatt, X. Huai, J. Liu, B. Singh, K.-M. Kim, R. M. Fernandes, P. Cardon, L. Zhao, T. T. Tran, B. A. Frandsen, K. S. Burch, F. Liu, and H. Ji, $\text{La}_2\text{O}_3\text{Mn}_2\text{Se}_2$: A correlated insulating layered d-wave altermagnet, *Phys. Rev. Mater.* **9**, 024402 (2025).
- [49] R. B. Regmi, H. Bhandari, B. Thapa, Y. Hao, N. Sharma, J. McKenzie, X. Chen, A. Nayak, M. El Gazzah, B. G. Márkus, L. Forró, X. Liu, H. Cao, J. F. Mitchell, I. I. Mazin, and N. J. Ghimire, Altermagnetism in the layered intercalated transition metal dichalcogenide CoNb_4Se_8 , *Nat. Commun.* **16**, 4399 (2025).
- [50] N. Dale, O. A. Ashour, M. Vila, R. B. Regmi, J. Fox, C. W. Johnson, A. Fedorov, A. Stibor, N. J. Ghimire, and S. M. Griffin, Non-relativistic spin splitting above and below the Fermi level in a g -wave altermagnet, [arXiv:2411.18761](https://arxiv.org/abs/2411.18761) (2024).
- [51] L. Šmejkal, J. Sinova, and T. Jungwirth, Emerging Research Landscape of Altermagnetism, *Phys. Rev. X* **12**, 040501 (2022).
- [52] I. I. Mazin, Notes on altermagnetism and superconductivity, [arXiv:2203.05000](https://arxiv.org/abs/2203.05000) (2022).
- [53] D. Zhu, Z.-Y. Zhuang, Z. Wu, and Z. Yan, Topological superconductivity in two-dimensional altermagnetic metals, *Phys. Rev. B* **108**, 184505 (2023).
- [54] S. Hong, M. J. Park, and K.-M. Kim, Unconventional p -wave and finite-momentum superconductivity induced by altermagnetism through the formation of bogoliubov fermi surface, *Phys. Rev. B* **111**, 054501 (2025).
- [55] D. Chakraborty and A. M. Black-Schaffer, Zero-field finite-momentum and field-induced superconductivity in altermagnets, *Phys. Rev. B* **110**, L060508 (2024).
- [56] A. Bose, S. Vadrnais, and A. Paramekanti, Altermagnetism and superconductivity in a multiorbital $t - J$ model, *Phys. Rev. B* **110**, 205120 (2024).
- [57] S.-B. Zhang, L.-H. Hu, and T. Neupert, Finite-momentum Cooper pairing in proximitized altermagnets, *Nat. Commun.* **15**, 1801 (2024).
- [58] K. Mæland, B. Brekke, and A. Sudbø, Many-body effects on superconductivity mediated by double-magnon processes in al-

- termagnets, *Phys. Rev. B* **109**, 134515 (2024).
- [59] K. Parshukov and A. P. Schnyder, Exotic superconducting states in altermagnets, [arXiv:2507.10700](https://arxiv.org/abs/2507.10700) (2025).
- [60] J. Linder and A. V. Balatsky, Odd-frequency superconductivity, *Rev. Mod. Phys.* **91**, 045005 (2019).
- [61] E. H. Lieb, Two theorems on the Hubbard model, *Phys. Rev. Lett.* **62**, 1201 (1989).
- [62] D. S. Antonenko, R. M. Fernandes, and J. W. F. Venderbos, Mirror Chern Bands and Weyl Nodal Loops in Altermagnets, *Phys. Rev. Lett.* **134**, 096703 (2025).
- [63] T. Jungwirth, R. M. Fernandes, E. Fradkin, A. H. MacDonald, J. Sinova, and L. Smejkal, Altermagnetism: an unconventional spin-ordered phase of matter, [arXiv:2411.00717](https://arxiv.org/abs/2411.00717) (2024).
- [64] M. R. Slot, T. S. Gardenier, P. H. Jacobse, G. C. P. van Miert, S. N. Kempkes, S. J. M. Zevenhuizen, C. M. Smith, D. Vanmaekelbergh, and I. Swart, Experimental realization and characterization of an electronic Lieb lattice, *Nat. Phys.* **13**, 672 (2017).
- [65] W. Wu, S. Sun, C. S. Tang, J. Wu, Y. Ma, L. Zhang, C. Cai, J. Zhong, M. V. Milošević, A. T. S. Wee, and X. Yin, Realization of a 2D Lieb Lattice in a Metal-Inorganic Framework with Partial Flat Bands and Topological Edge States, *Adv. Mater.* **36**, 2405615 (2024).
- [66] M. Dürrnagel, H. Hohmann, A. Maity, J. Seufert, M. Klett, L. Klebl, and R. Thomale, Altermagnetic Phase Transition in a Lieb Metal, *Phys. Rev. Lett.* **135**, 036502 (2025).
- [67] N. Kaushal and M. Franz, Altermagnetism in modified Lieb lattice Hubbard model, [arXiv:2412.16421](https://arxiv.org/abs/2412.16421) (2024).
- [68] N. Ni, E. Climent-Pascual, S. Jia, Q. Huang, and R. J. Cava, Physical properties and magnetic structure of the layered oxyelenide $\text{La}_2\text{O}_3\text{Mn}_2\text{Se}_2$, *Phys. Rev. B* **82**, 214419 (2010).
- [69] G. M. Eliashberg, Interactions between electrons and lattice vibrations in a superconductor, *Zh. Eksp. Teor. Fiz.* **38**, 966 (1960), [*Sov. Phys. JETP* **11**, 696 (1960)].
- [70] G. M. Eliashberg, Temperature Green's function for electrons in a superconductor, *Zh. Eksp. Teor. Fiz.* **39**, 1437 (1960), [*Sov. Phys. JETP* **12**, 1000 (1961)].
- [71] P. M. R. Brydon, S. Das Sarma, H.-Y. Hui, and J. D. Sau, Odd-parity superconductivity from phonon-mediated pairing: Application to $\text{Cu}_x\text{Bi}_2\text{Se}_3$, *Phys. Rev. B* **90**, 184512 (2014).
- [72] I. Schnell, I. I. Mazin, and A. Y. Liu, Unconventional superconducting pairing symmetry induced by phonons, *Phys. Rev. B* **74**, 184503 (2006).
- [73] F. Schrodri, P. M. Oppeneer, and A. Aperis, Unconventional superconductivity mediated solely by isotropic electron-phonon interaction, *Phys. Rev. B* **104**, L140506 (2021).
- [74] J. Linder and J. W. A. Robinson, Superconducting spintronics, *Nat. Phys.* **11**, 307 (2015).
- [75] M. Lax, *Symmetry Principles in Solid State and Molecular Physics* (Wiley, New York, 1974).
- [76] H. Bruus and K. Flensberg, *Many-Body Quantum Theory in Condensed Matter Physics: An Introduction* (Oxford University Press, Oxford, 2004).
- [77] J. N. Kløgetvedt, Topological Magnon-Phonon Hybrid Excitations and Hall Effects in Two-Dimensional Ferromagnets, Master thesis, Norwegian University of Science and Technology, <https://hdl.handle.net/11250/3097131> (2023).
- [78] E. Syljuåsen, Transverse quantum transport in multiband Bose-systems, Master thesis, Norwegian University of Science and Technology, <https://hdl.handle.net/11250/3155941> (2024).
- [79] E. Thingstad, A. Kamra, J. W. Wells, and A. Sudbø, Phonon-mediated superconductivity in doped monolayer materials, *Phys. Rev. B* **101**, 214513 (2020).
- [80] J. Bardeen and D. Pines, Electron-Phonon Interaction in Metals, *Phys. Rev.* **99**, 1140 (1955).
- [81] J. R. Schrieffer and P. A. Wolff, Relation between the Anderson and Kondo Hamiltonians, *Phys. Rev.* **149**, 491 (1966).
- [82] E. Thingstad, *Collective effects in low-dimensional systems with coupled quasiparticles*, *Ph.D. thesis*, NTNU, Norway (2021).
- [83] K. Mæland, *Many-body effects and topology in magnets and superconductors*, *Ph.D. thesis*, NTNU, Norway (2024).
- [84] P. O. Sukhachov, F. von Oppen, and L. I. Glazman, Andreev Reflection in Scanning Tunneling Spectroscopy of Unconventional Superconductors, *Phys. Rev. Lett.* **130**, 216002 (2023).
- [85] P. O. Sukhachov, F. von Oppen, and L. I. Glazman, Tunneling spectra of impurity states in unconventional superconductors, *Phys. Rev. B* **108**, 024505 (2023).
- [86] G. D. Mahan, *Many-Particle Physics* (Springer, New York, 2000).